Mechanism and kinetics of the n-propyl bromide and OH reaction using integrated ab initio methods and variational transition-state theory

ARTICLE *in* JOURNAL OF MOLECULAR STRUCTURE THEOCHEM · JUNE 2004

Impact Factor: 1.37 · DOI: 10.1016/j.theochem.2004.04.019

3 AUTHORS:

Cipriano Rangel
Universidad de Extremadura
27 PUBLICATIONS **321** CITATIONS
SEE PROFILE

Marta Navarrete
Spanish National Research Council
22 PUBLICATIONS **1,235** CITATIONS
SEE PROFILE

Jose C Corchado
Universidad de Extremadura
118 PUBLICATIONS **3,296** CITATIONS
SEE PROFILE

ELSEVIER

Journal of Molecular Structure (Theochem) 679 (2004) 207–224

THEO CHEM

www.elsevier.com/locate/theochem

Mechanism and kinetics of the *n*-propyl bromide and OH reaction using integrated ab initio methods and variational transition-state theory

C. Rangel, M. Navarrete, J.C. Corchado, J. Espinosa-García*

Departamento de Química Física, Facultad de Ciencias, Universidad de Extremadura, 06071 Badajoz, Spain

Received 16 February 2004; revised 12 April 2004; accepted 13 April 2004

Abstract

The reaction of the OH radical with *n*-propyl bromide, $^{\gamma}CH_3^{\beta}CH_2^{\alpha}CH_2Br$, was studied by integrated ab initio electronic structure methods and variational transition-state theory with multidimensional tunneling. The mechanism of the reaction involves three channels, corresponding to hydrogen abstractions from three different carbon sites, α, β, and γ. While the attack on the α and β carbons proceeds via hydrogen-bonded complexes in the entrance and exit channels, the reaction on the γ carbon proceeds directly without intermediate complexes. For each hydrogen abstraction reaction, all the stationary points (reactants, products, saddle point, and complexes) were located and characterized. The respective intrinsic reaction paths were independently constructed using integrated ab initio methods, and the rate constants were independently calculated for the temperature range 200–2000 K using variational transition-state theory with multidimensional tunneling. The partial (α, β, and γ) and total rate constants show curvature of the Arrhenius plot in agreement with the experimental evidence, indicating the importance of the tunneling effect. Finally, the branching ratios were analysed, showing a change of the abstraction site from β to γ as temperature went up.

Keywords: *n*-Propyl bromide; OH free radical; Ab initio integrated methods; Variational transition-state theory; Tunneling effect; Kinetics and mechanism

1. Introduction

The atmospheric chemistry of bromine-containing molecules and free radicals attracted great attention in the 1990s because of the role that bromine atoms play in the catalytic destruction of the Earth's protective ozone layer in the stratosphere [1,2]. In recent years, there has been a renewal of interest following the recognition that the tropospheric reactions of Br atoms and BrO_x radicals are significantly more important than they were thought before, particularly in the Arctic region and marine boundary layers [3–5].

Although bromine is emitted into the atmosphere mostly in the form of CH_3Br from both anthropogenic and natural sources, in much smaller concentration CH_2ClBr and $CH_3CH_2CH_2Br$ (1-bromopropane, *n*-propyl bromide, *n*PB) are also permanent bromine constituents of the troposphere. Last is an industrial cleaning solvent, which has been proposed as a CFC substitute because of its short residence times in the atmosphere. These brominated molecules release bromine atoms and other bromine-containing free radicals into the air through a series of degradation processes, which are initiated by the reactions with hydroxyl radicals. Understanding the chemistry of these brominated molecules and radicals in the atmosphere requires a knowledge of their thermochemistry and kinetics. The kinetic parameters for many of the atmospheric reactions of brominated molecules are, however, not well known or not available at all. Several laboratories [6–12] found that, because of the reaction with hydroxyl radicals, *n*PB presents a short atmospheric lifetime, in the range 8–34 days.

Experimentally, the title reaction has been widely studied [6–15]. Of the more recent kinetics studies, Herndon et al. [14] determined the rate coefficient to be $k(T) = 9.1 \times 10^{-14}\ T^{0.5} \exp(-157/T)$ over the temperature range 220–380 K, using pulsed photolysis–pulsed laser induced fluorescence (PP-PLIF), with a value $k(298\ \mathrm{K}) = (8.7 \pm 0.4)\ 10^{-13}\ \mathrm{cm^3\ molecule^{-1}\ s^{-1}}$. Later, Gilles et al. [11] reported a value of $k(T) = 6.6 \times 10^{-18}\ T^2 \exp(-154/T)$ using a similar technique over the temperature range 230–360 K, with a value $k(298\ \mathrm{K}) = (9.53 \pm 0.37)\ 10^{-13}\ \mathrm{cm^3\ molecule^{-1}\ s^{-1}}$, i.e. 10% greater. These workers also reported for the first time the branching ratios

* Corresponding author. Tel.: +34-92-428-9684; fax: +34-92-427-5576.
E-mail address: joaquin@unex.es (J. Espinosa-García).

0166-1280/$ - see front matter © 2004 Elsevier B.V. All rights reserved.
doi:10.1016/j.theochem.2004.04.019

of the attack of the OH at different sites along the carbon chain ($^{\gamma}CH_3^{\beta}CH_2^{\alpha}CH_2Br$). At 298 K, the values are: $k_\alpha/k = 0.32 \pm 0.08$, $k_\beta/k = 0.56 \pm 0.04$, and $k_\gamma/k = 0.12 \pm 0.08$. This behaviour agrees with the strength of the C–H breaking bond (α, β, and γ positions) measured from their bond dissociation energies ($BDE_{298\ K}$): 98.6 ± 1.2, 96.0 ± 2.1, and 101.6 ± 1.0 kcal mol^{-1}, respectively [16]. Finally, Kurylo et al. [12] measured the rate coefficient using the flash photolysis resonance fluorescence technique over the temperature range 210–480 K: $k(T) = 2.99\ 10^{-13}\ (T/298)^{2.79}\ \exp(+369/T)$, with a value $k(298\ K) = (10.1 \pm 0.15)10^{-13}$ cm^3 molecule^{-1} s^{-1}, i.e. slightly greater than the previous measures.

Despite its importance in atmospheric chemistry, *n*-propyl bromide has until recently been the subject of relatively few high-level theoretical studies. The reason is the computational effort demanded by such a large electronic system as the bromine atom. To the best of our knowledge, the only theoretical work is that of Gilles et al. [11]. They located the transition states for OH attack at the α, β, and γ sites of the carbon chain and determined the barrier heights, using the Gaussian-3 (G3) method [17,18]. However, they did not perform theoretical kinetics studies on the title reaction.

The kinetic and dynamic study of reactions involving large compounds (molecules and free radicals) represent an exciting challenge to the theoretical chemist because the application of high-level calculations is prohibitive. To circumvent this problem, i.e. large compounds/high-level, two alternatives, mainly, can be used. One involves Density Functional Theory (DFT) [19–23]. It is well known that DFT calculations or hybrid DFT calculations that mix in variable proportions Hartree-Fock exchange yield reasonable geometries and vibrational frequencies [24], atomization energies [25], and enthalpies of formation [26]. However, when breaking–forming bonds are involved in the transition state zone, DFT or hybrid DFT fail to perform well [27–35], and generally underestimate the barrier height by several kcal mol^{-1}. In sum, the accuracy limitation of the DFT and hybrid DFT approaches dissuade one from using them for the reaction-path description.

An interesting and economic group of alternatives for the problem of large molecules and high-level calculations are the integrated methods, which describe different parts of the large system with different theoretical approaches [36–54]. The main goal is to reproduce the results of a high-level theoretical calculation for a large, *complete* system, by dividing it into two parts: a small *model* system (which is the most active site, where the breaking–forming bonds are involved), and the *rest* of the molecular system. Different levels of theory are applied to these two parts, a higher-level for the *model* system and a lower-level for the *complete* system. The first studies were devoted to the analysis of stationary points with special attention to stable molecules. Comparatively, however, far less effort has been devoted to the study of the performance of the integrated methods in describing saddle points [44,54–59] and reaction paths [54,56–59]. Recently, our group has extended the idea of the integrated methods to the reaction-path construction in a chemical reaction and thence to studying the kinetics and dynamics [54,60,61]. We concluded that the integrated methods reproduce the behaviour of a benchmark calculation for kinetic and dynamic properties along the reaction-path, and that the success of these methods is mainly due to the higher-level 'model' system description, showing little dependence on which 'low-level' was used in the computation.

In this work our objectives are threefold. One is to study the '$CH_3CH_2CH_2Br + OH \rightarrow$ Products' hydrogen abstraction reaction in order to obtain kinetics information using canonical variational transition-state theory with multidimensional tunneling. The second is to continue investigating the performance of the integrated methods, extending the field of our previous studies [54,60,61] to competitive reactions. In particular we will use the integrated IMOMO method [41–47,53] to study the mechanism of the attack of the OH free radical, analysing theoretically the possible reaction pathways with the three different attack sites considered separately. Finally, the third is to extend the low temperature range of atmospheric interest to higher temperatures, which are of interest in combustion chemistry and have not been experimentally studied. In Section 2 we give the theoretical methods and computational details, in Section 3 the results and a discussion, and in Section 4 our conclusions.

2. Methods and computational details

2.1. Electronic structure calculations

Geometry, energy, and first and second energy derivatives of all stationary points were calculated using the integrated IMOMO method [41–47,53] implemented in the GAUSSIAN 98 program [62].

The 'complete' system (CS) is the hydrogen abstraction reaction from the three different sites along the carbon chain

$$CH_3CH_2CH_2Br + OH \rightarrow CH_3CH_2CHBr + H_2O \qquad (R_\alpha)$$

$$CH_3CH_2CH_2Br + OH \rightarrow CH_3CHCH_2Br + H_2O \qquad (R_\beta)$$

$$CH_3CH_2CH_2Br + OH \rightarrow CH_2CH_2CH_2Br + H_2O \qquad (R_\gamma)$$

which are calculated at the low MO level (LL) and are denoted (CS,LL).

For each OH approach the respective model system (MS), or inner layer, is the most active site of the reaction. They are

$$CH_3Br + OH \rightarrow CH_2Br + H_2O \qquad (R_{m\alpha})$$

$$CH_4 + OH \rightarrow CH_3 + H_2O \qquad (R_{m\beta})$$

$$CH_4 + OH \rightarrow CH_3 + H_2O \qquad (R_{m\gamma})$$

which are calculated at a higher MO level (HL) and are denoted (MS,HL). Note that in the IMOMO approach it is necessary to add 'link' atoms onto the CH_x fragment in the model system to ensure a saturated valence structure. Thus, for the R_α and R_γ reactions, where a primary carbon is involved, only one link atom is necessary ($H-CH_2Br + OH$ and $H\text{-}CH_3 + OH$, respectively), while for the R_β reaction, where the active site is located on a secondary carbon, two link atoms are necessary ($H-CH_2-H + OH$).

For each reaction pathway, the final integrated IMOMO method is then denoted (MS,HL): (CS,LL), and the energy of the *complete* system is approximated by

$$E_{CS}(I) = E_{CS}(LL) - E_{MS}(LL) + E_{MS}(HL) \quad (1)$$

where (I) denotes integrated level, and only one set of structural parameters is used to get the energies. Stated in this way, Eq. (1) considers the integrated calculation as the inclusion of higher-level effects in a lower-level calculation for the *complete* system [51].

In this present work, for the geometry optimization and frequency calculation, the MP2 = FULL/6-31G(d,p) level (second order Møller–Plesset perturbation theory with full electron correlation) was chosen as HL, while the HF/6-31G level (Hartree-Fock) was selected as LL. The choice of this low-level is justified by two reasons: first, by the conclusions of earlier work [49,54,55] that the integrated scheme shows little dependence on which low-level is used; and second, because each reaction path requires information of energy, first and second derivatives for hundreds of points, which implies than more than 1000 Hessians needed to be determined for the present calculations. Such calculations require an enormous amount of time, which was reduced by choosing an inexpensive low level. The integrated level is then

$$\text{MP2} = \text{FULL/6-31G(d,p)} : \text{HF/6-31G}$$

where the colon separated pair (X_1:X_2) denotes the integrated level used: X_1 is the higher-level for the *model* system, or inner layer, and X_2 is the lower-level for the *complete* system, or outer layer. This level is denoted as Level 0.

At a second step, to improve the energy description of the stationary points, a single-point calculation is made at higher-levels, i.e. calculation of the energy at a higher integrated level using the geometry optimized in the previous step

Level I Using the geometries optimized at Level 0, a single-point calculation is made with a better description of the model system using the CCSD(T) [63] (coupled-cluster approach with single and double substitutions including a perturbational estimate of connected triple substitutions) with the 6-311++G(2d,p) basis set. This energy is denoted as

$$\text{CCSD(T)/6-311++G(2d,p)} : \text{HF/6-31G//MP2} = \text{FULL/6-31G(d,p)} : \text{HF/6-31G}$$

where the double slash (X//Y) denotes geometry optimization at level Y and energy calculated at level X, both integrated levels.

Level II Continuing with the CCSD(T) approach and a more extended basis set, 6-311++G(2d,2p), we also augmented the MO level to describe the model reaction, namely, MP2 = FULL/6-31G(d,p). This integrated energy is denoted as

$$\text{CCSD(T)/6-311++G(2d,2p)} : \text{MP2} = \textit{FULL}/6\text{-}31G(d,p)//\textit{MP2} = \textit{FULL}/6\text{-}31G(d,p) : \textit{HF}/6\text{-}31G$$

2.2. Dynamics calculations

For each reaction pathway independently (R_α, R_β, and R_γ) using the Level 0, the 'intrinsic reaction coordinate' (IRC), or minimum energy path (MEP), is constructed starting from the saddle point geometry and going downhill to both the asymptotic reactant and product channels in mass-weighted Cartesian coordinates with a gradient step size of 0.02 bohr $amu^{1/2}$. The Hessian matrix is evaluated at every point along the reaction-path, always avoiding the undesirable reorientations of molecular geometries. Along each MEP the reaction coordinate, s, is defined as the signed distance from the saddle point, with $s > 0$ referring to the product side. In the rest of the work the units of s are bohr, and the reduced mass to scale the coordinates [64] is set to 1 amu. This has no effect on calculated observables, but it does affect the magnitude of s in plots used for interpretative purposes.

Along each MEP, a generalized normal-mode analysis is performed projecting out frequencies at each point along the path [65]. With this information, the respective ground-state vibrationally adiabatic potential curve is calculated

$$V_a^G(s) = V\text{MEP}(s) + \varepsilon_{int}^G(s) \quad (2)$$

where $V_{MEP}(s)$ is the classical energy along each MEP with its zero energy at the reactants ($s = -\infty$), and $\varepsilon_{int}^G(s)$ is the zero-point energy at s from the generalized normal-mode vibrations orthogonal to the reaction coordinate.

Finally, the energies, vibrational frequencies, geometries, and gradients along each MEP are used to estimate the respective rate constants by using variational transition state theory (VTST). Thermal rates are calculated using the canonical variational theory [66,67] (CVT) approach which locates the dividing surface between reactants and products

at a point $s*^{CVT}(T)$ along the reaction path that minimizes the generalized TST rate constants, $k^{GT}(T,s)$ for a given temperature T. Thermodynamically, this is equivalent to locating the transition state at the maximum $\Delta G^{GT,o}[T, s*^{CVT}(T)]$ of the free energy of activation profile $\Delta G(T,s)$ [66,67]. Thus, the thermal rate constant will be given by

$$k^{CVT}(T) = \sigma \frac{k_B T}{h} K^o \exp[-\Delta G(T, s^{*,CVT})/k_B T] \quad (3)$$

with k_B being Boltzmann's constant, h Planck's constant, σ the symmetry factor (the number of equivalent reaction paths), and K^o the reciprocal of the standard-state concentration, taken as 1 molecule cm^{-3}.

The present work used the general polyatomic rate constants program GAUSSRATE [68] which is an implementation based on the GAUSSIAN 98 [62] and the POLYRATE [69] programs. Note that the current version of GAUSSRATE does not allow one to use the IMOMO method implemented in the GAUSSIAN 98 program. Therefore, in the present work a locally modified version of GAUSSRATE was used. Since integrated methods are used, this version of GAUSSRATE is equivalent to our RAIL method [54]. The rotational partition functions were calculated classically and the vibrational modes were treated as quantum-mechanical separable harmonic oscillators, with the generalized normal-modes defined in redundant curvilinear coordinates [70,71]. The curvilinear coordinates chosen were all the possible bond lengths and angles. The advantage of curvilinear coordinates (non-linear functions of Cartesian coordinates) over rectilinear ones (linear functions of Cartesian coordinates) is that in some cases the lowest bending frequencies have unphysical imaginary values over a wide range of the reaction coordinate using rectilinear coordinates, whereas these frequencies are real over the whole of the reaction-path using curvilinear coordinates. This behaviour has been observed in other hydrogen abstraction reactions [72–74]. The calculation of electronic partition functions included the two electronic states for the OH reactant, with 140 cm^{-1} splitting. For the tunneling contribution, as information is only available on the reaction-path, centrifugal-dominant small-curvature tunneling (SCT) [75] was used. Methods for large curvature cases have been developed [76], but they require more information about the PES than was determined in the present study.

3. Results and discussion

3.1. Mechanism of reaction

When the hydroxyl radical attacks nPB, three approaches (R_α, R_β, and R_γ) are possible, which will be analysed independently. Fig. 1 shows a schematic

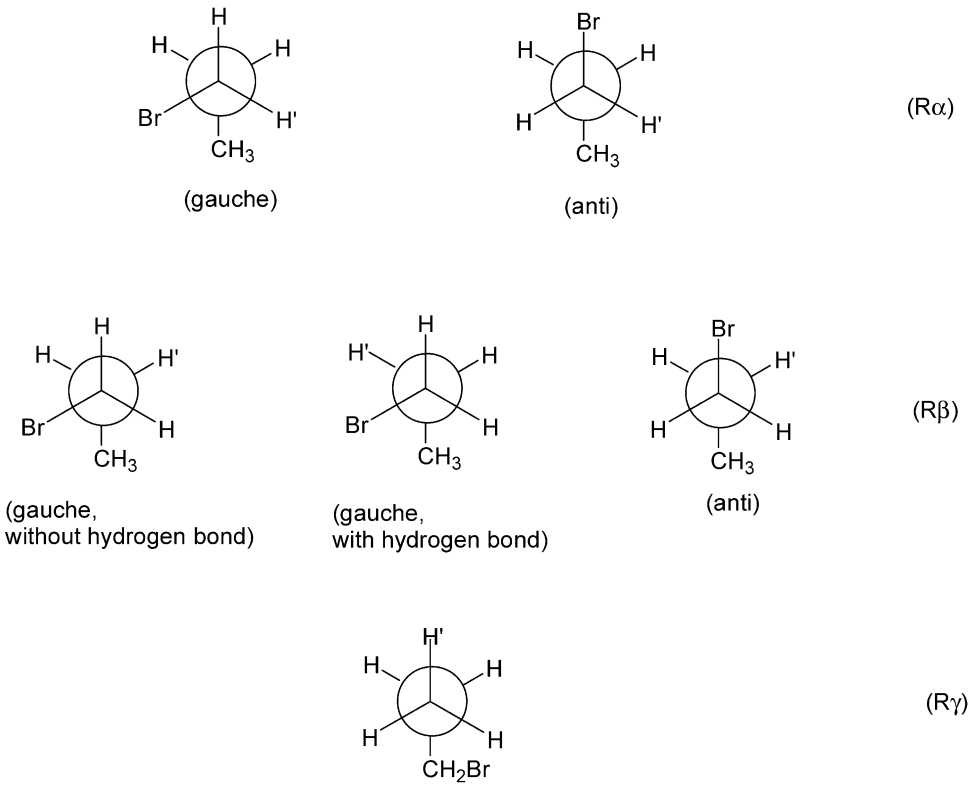

Fig. 1. Schematic representation of the three OH attacks, where the different conformations have been considered. H′ is the hydrogen being abstracted. The possible hydrogen bond refers to the bond of the OH free radical with the bromine atom.

representation including the different conformations, *gauche* and *anti*.

We shall begin by analysing the hydrogen abstraction reaction on the H′ atom in the R_α reaction, where two conformers (*gauche* and *anti*) are possible. These conformations are similar in energy with the *anti* form slightly more stable (0.02 kcal mol^{-1}). Because of this similarity, only the *anti* conformer will be calculated. On this reaction path, the reaction of the OH radical with the molecule proceeds via a weakly reactant hydrogen-bonded complex (denoted CR_α), a saddle point (denoted SP_α) and a product hydrogen-bonded complex (denoted CP_α), as shown in Fig. 2. The first stationary point (CR_α) is a complex stabilized by two hydrogen bonds, with bond distances O···H′ of 2.620 Å and Br···H of 2.556 Å. The other bond lengths and bond angles are very close to those of the separated reactants. Subsequently, shortening of the O···H′ interatomic distance led us to a second stationary point, which is a saddle point (SP_α). The length of the bond that is broken (C–H′) increases by 10% and the length of the bond that is formed (H′–O) increases by 33%, with respect to *n*PB and H_2O, respectively. Therefore, the reaction of the OH radical with the molecule proceeds via an 'early' transition state, which is the expected behaviour that would follow from Hammond's postulate [77], since the reaction is exothermic (see Table 4). Finally, a third stationary point was found on the product side, which is also a complex stabilized by two hydrogen bonds (CP_α).

The three stationary points (CR_α, SP_α and CP_α) were all identified by means of the eigenvalues of the Hessian matrix: the complexes are minima on the potential energy surface with all frequencies real, and the saddle point has one and only one negative eigenvalue and, therefore, one imaginary frequency (Table 1). The corresponding eigenvector is associated with the broken and formed bonds. The small geometrical variations between the complexes

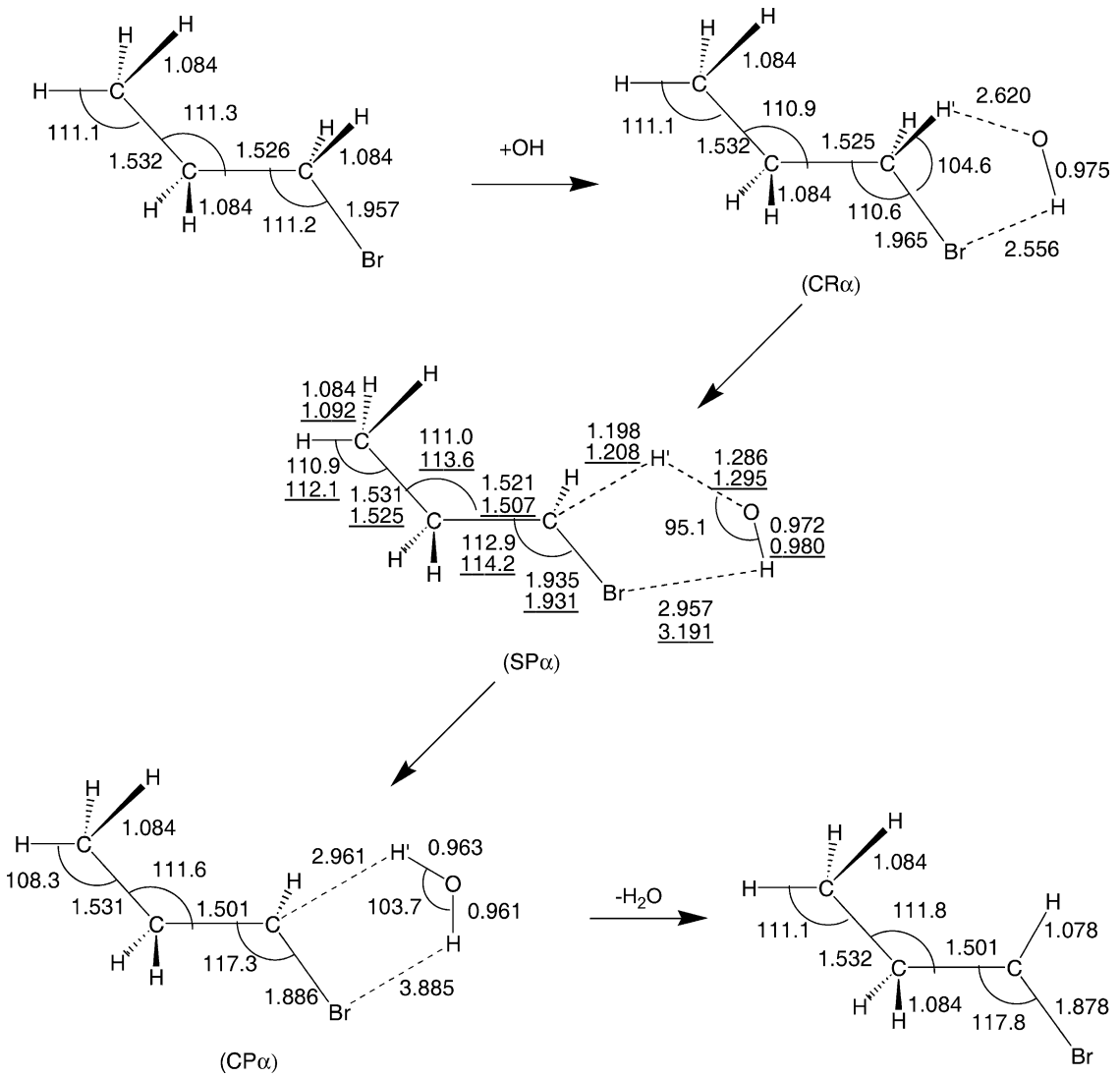

Fig. 2. Optimized stationary point geometries at Level 0 for the R_α reaction, *anti* conformer. CR_α, reactive complex; SPα, saddle point; CP_α, product complex. H′ is the hydrogen being abstracted. Bonds in Å and angles in degrees. For comparison, underlined are the values for the 'complete' system, independent of the IMOMO approach, optimized at the MP2 = FULL/6-31G(d) level, from Ref. [11].

Table 1
Harmonic vibrational frequencies (cm^{-1}) and zero-point energy (ZPE, kcal mol^{-1}) for the R_α reaction at the integrated Level 0

R^a	CR_α	SP_α	CP_α	P
3285	3786	3832	4017	3320
3263	3294	3274	3885	3266
3261	3269	3266	3323	3265
3243	3264	3247	3270	3205
3215	3247	3233	3266	3193
3197	3217	3207	3222	3173
3188	3204	3192	3194	1659
1665	3190	1664	3179	1656
1657	1665	1657	1697	1644
1653	1657	1651	1659	1582
1582	1652	1583	1656	1517
1545	1583	1514	1647	1411
1511	1545	1471	1582	1324
1447	1511	1424	1528	1234
1356	1450	1350	1420	1197
1323	1359	1291	1320	1123
1215	1329	1227	1237	995
1128	1218	1182	1204	874
1111	1139	1112	1122	754
968	1110	982	995	454
924	968	940	882	340
792	931	858	747	250
705	801	825	476	227
333	698	700	377	84
248	452	657	339	
229	337	336	249	
118	332	257	229	
	249	233	224	
	228	200	128	
	144	119	108	
	131	94	97	
	71	81	69	
	24	2224 i	23	
ZPE				
63.13	70.12	66.71	69.15	53.96

[a] OH vibrational frequency at the MP2 = FULL/6-31G(d,p) level: 3846 cm^{-1} (ZPE = 5.50 kcal mol^{-1}), compared with the experimental value 3735 cm^{-1} from Ref. [82].

and reactant or product cause very few changes in the harmonic vibrational frequencies of the complexes. The lowest values of the complexes correspond to restricted motions that previously were free rotations and translations of the reactants or products, and these vibrational modes would be expected to have very low frequencies.

Next, we shall analyse the second approach of the OH radical, i.e. the hydrogen abstraction reaction of the hydrogen atoms on the C_β (R_β reaction), which also presents two conformers, *gauche* and *anti*. In this case, in the *gauche* form, when the OH approaches the molecule the two abstractable hydrogens on C_β are not equivalent. In one approach there is the possibility of a hydrogen bond (HB) with bromine (*gauche* with HB in Fig. 1), while in the other this possibility disappears (*gauche* without HB in Fig. 1). The *anti* and *gauche* conformers are similar in energy with the *gauche* form slightly more stable (0.1 kcal mol^{-1}). For the *gauche* with HB and *anti* conformers, the reactions evolve in a way similar to the R_α reaction, and are shown in Figs. 3 and 4, respectively. In both cases, a reactant hydrogen-bonded complex (denoted CR_β) is found, stabilized by two hydrogen bonds, with the other geometric parameters being very close to those of the separated reactants. Second, there is a saddle point (SP_β) with increases in the lengths of the bonds broken/formed that are the same as in the SP_α, 10 and 33%, respectively, i.e. corresponding to an early transition state. Note that while for this reaction the saddle points form six-membered ring structures, for the R_α reaction the saddle point forms a five-membered ring structure. Finally, there is a third stationary point in the product valley, which is similar to that found in the R_α reaction, the CP_β complex stabilized by only one hydrogen bond. Note that for both conformations (*anti* and *gauche* with HB), after the saddle point on the reaction path, the secondary carbon changes its sp^3 hybridisation to sp^2, and for the *anti* conformation, the $^\beta C-{}^\alpha C$ bond also rotates. This originates, firstly, that the bromine atom loses its original *anti* conformation and secondly, that its bond with the α carbon is weaker for both conformations.

For the *gauche* without HB conformer, the reaction evolves directly through a saddle point, without intermediary complexes (Fig. 5). The lengths of the bonds broken/formed at the saddle point are similar to the earlier cases (9 and 37%, respectively).

For all possibilities of the R_β reaction, the vibrational analysis confirmed the nature of these stationary points (Table 2). Thus, CR_β and CP_β are minima on the potential energy surface, and SP_β has one and only one imaginary frequency associated to the broken/formed bonds. The absolute values, 2015, 2014 and 1826 cm^{-1} for the *gauche* with HB, *anti*, and *gauche* without HB, respectively, are lower than the corresponding value for SP_α (2224 i cm^{-1}).

Next, we shall analyse the third approach of the OH radical, R_γ. In this case, the three hydrogen atoms of the methyl group can be considered equivalent. At the Level 0, this reaction evolves directly from reactants to products through a saddle point without intermediary complexes in the reactant or product channels (Fig. 6), as in the R_β reaction for the *gauche* without HB conformer. This result agrees with the theoretical studies for the CH_4 + OH model reaction [78–80]. Basch and Hoz [78] using ab initio calculations found a complex in the entrance channel that does not have the expected $CH_3-H\cdots OH$ geometry and is not on the IRC. Instead, the $CH_4\cdots HO$ geometry is preferred. More recently, Wheeler et al. [79] find experimentally a similar complex in the entrance channel. In the exit channel, Basch and Hoz find a complex $CH_3\cdots HOH$ that is so weak that it is not stable energetically after inclusion of the ZPE; i.e. this complex does not support any bound vibrational level. In the recent higher-level ab initio calculations of Masgrau et al. [80], the product complex is also found, but in this case is weakly bound at 0 K and higher

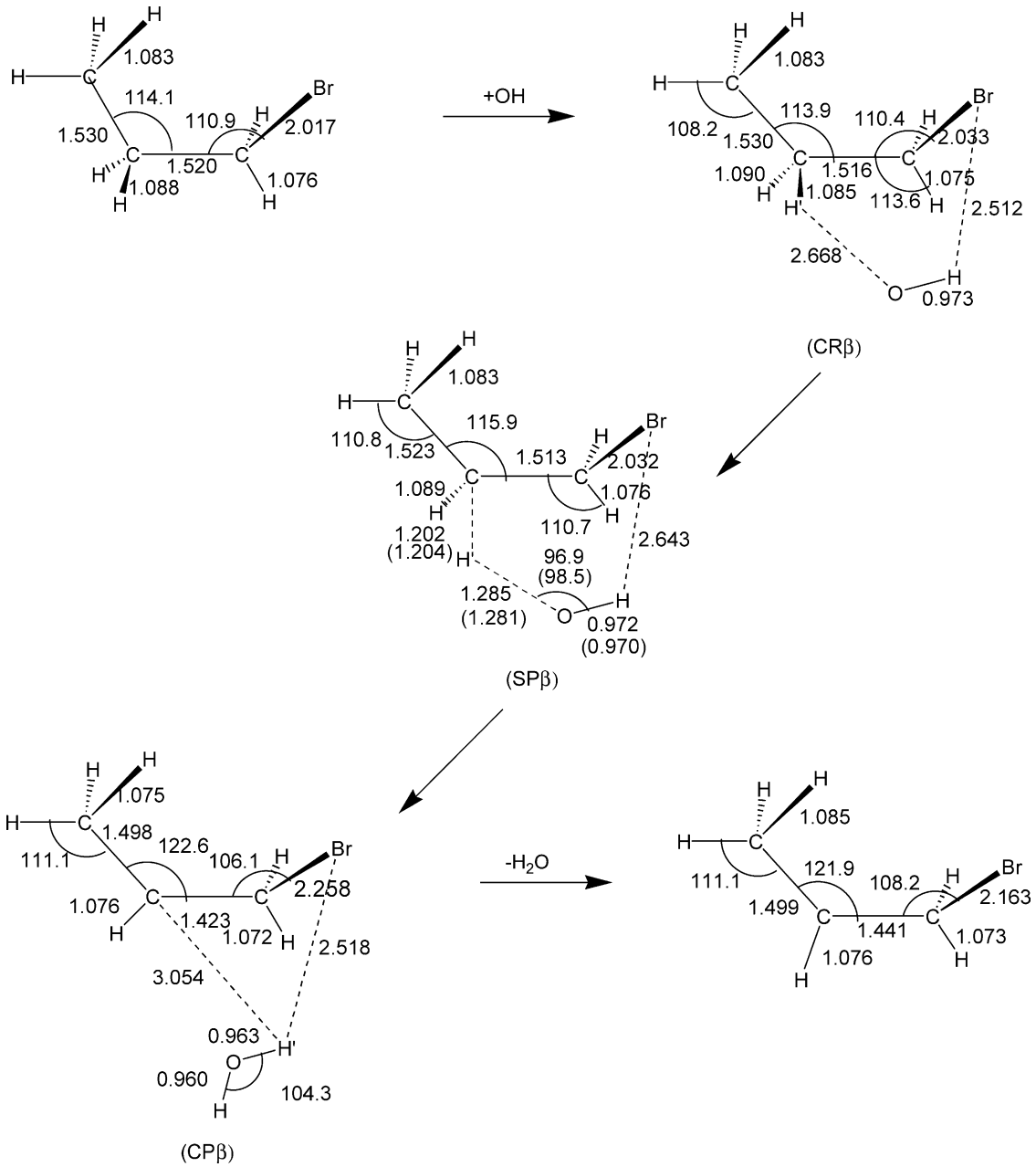

Fig. 3. Optimized stationary point geometries at Level 0 for the R_β reaction, *gauche* with hydrogen bond conformer. CR_β, reactive complex; SP_β, saddle point; CP_β, product complex. H′ is the hydrogen being abstracted. Bonds in Å and angles in degrees. For comparison, in parentheses are the values for the 'model' system, CH_4 + OH, independent of the IMOMO approach, optimized at the MP2 = FULL/6-31G(d,p) level.

temperatures. Moreover, when, for a more similar reaction, CF_3CH_3 + OH, our group [60] analysed the possibility of intermediate complexes in the entrance and exit channels, all the attempts with this integrated method, Level 0, proved unsuccessful.

At the saddle point for the R_γ reaction, where the bond that is broken (C–H′) increases by only 10%, the length of the bond that is formed (O–H′) increases by 34%, i.e. the transition state is also earlier. This behaviour agrees with the results found for the R_α and R_β reactions. The vibrational analysis confirmed the nature of this stationary point (Table 3), with one and only one imaginary frequency associated to the broken/formed bonds, having an absolute value of 1999 i cm^{-1}.

3.2. Relative energies

The changes in energy (ΔE) and enthalpy (ΔH, 0 and 298 K) of all stationary points relative to the reactants are listed in Table 4 for several integrated levels, together the Gilles et al.'s G3 results for comparison. Note that ΔH(0 K) is ΔE corrected with the zero-point energy, and ΔH(298 K) includes the thermal corrections at 298 K.

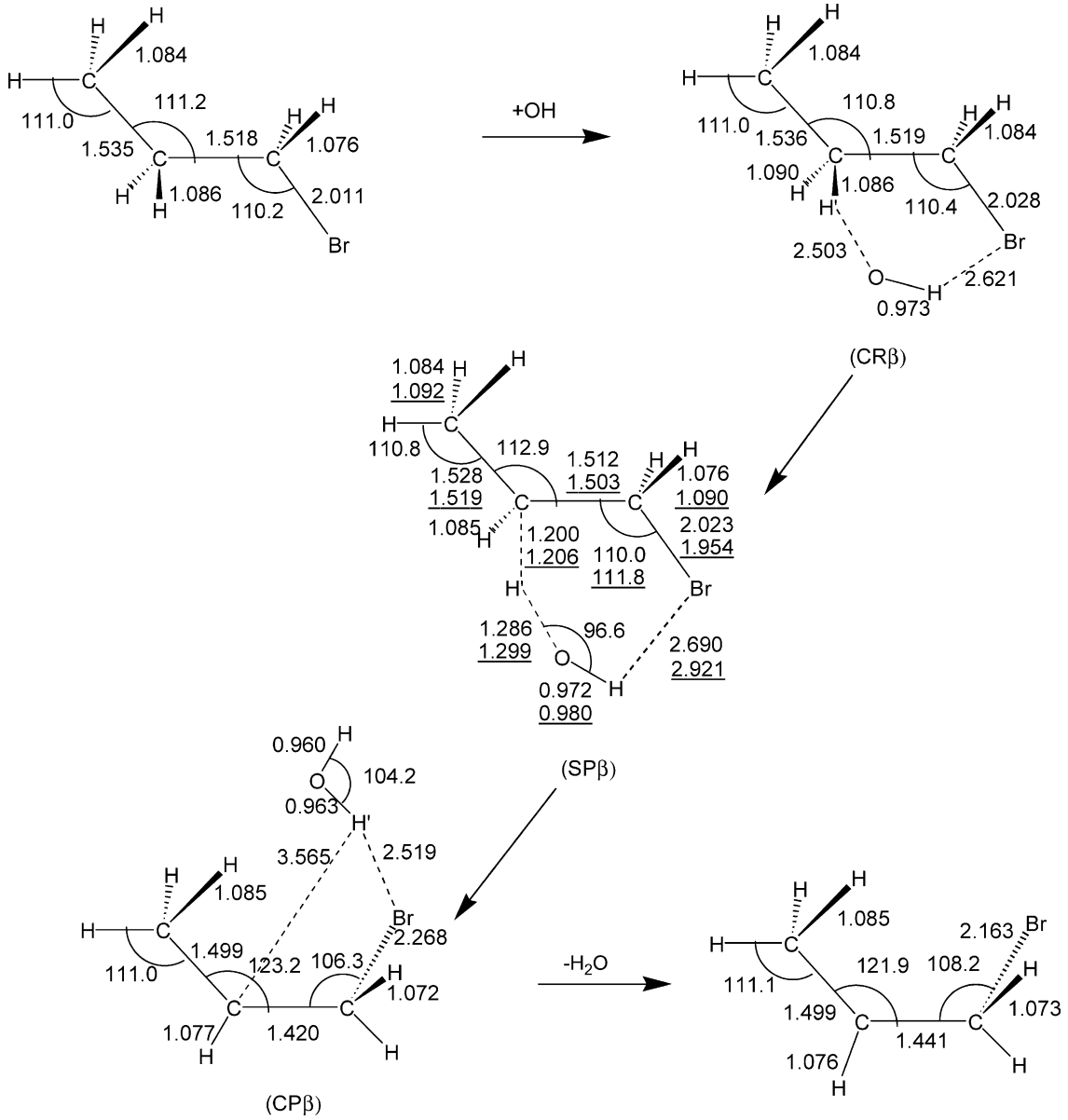

Fig. 4. Same as Fig. 3, but for the *anti* conformer. Underlined are the values for the 'complete' system at the MP2 = FULL/6-31G(d) level, from Ref. [11].

First, we analyse the enthalpy of reaction, which can be compared with those obtained from the reactants' and products' enthalpies of formation at 298 K. In the three reactions (R_α, R_β, and R_γ) all theoretical levels overestimate (more positive values) the experimental enthalpy of reaction, with differences in the range 3–5 kcal mol^{-1} at the highest Level II, with a narrower range (2–3 kcal mol^{-1}) when the experimental error bars are considered. Therefore, this is the associated error to the level (correlation + basis set). This result is not surprising because it is well known [83,84] that the CCSD(T) level has a tendency to overestimate the reaction energies of hydrogen abstraction reactions due to the slow convergence of the calculations with the dimensions of the basis sets. Note that even the very high ab initio G3 results of Gilles et al. [11] overestimate the experimental values by about 1 kcal mol^{-1}.

Let us now consider the hydrogen-bonded complexes. The reactive and product complexes (CR and CP) appear at an energy lower than that of the reactants, between 6 and 7 kcal mol^{-1}, and that of the products, between 5 and 8 kcal mol^{-1}, respectively. These stabilities diminish: (i) when the level of calculation rises, to between 3.7 and 6 kcal mol^{-1}, and between 3.9 and 6.5 kcal mol^{-1}, respectively, at Level II; (ii) when the zero-point energy (0 K) is included, to 2.3–4.3 and 2.4–4.4 kcal mol^{-1}, respectively; and (iii) when the thermal corrections (298 K) are included, to 1.9–4.1 and 1.7–4.0 kcal mol^{-1}, respectively. In general, the hydrogen-bonded complexes on the β (secondary) carbon are more stable than those on the α (primary) carbon.

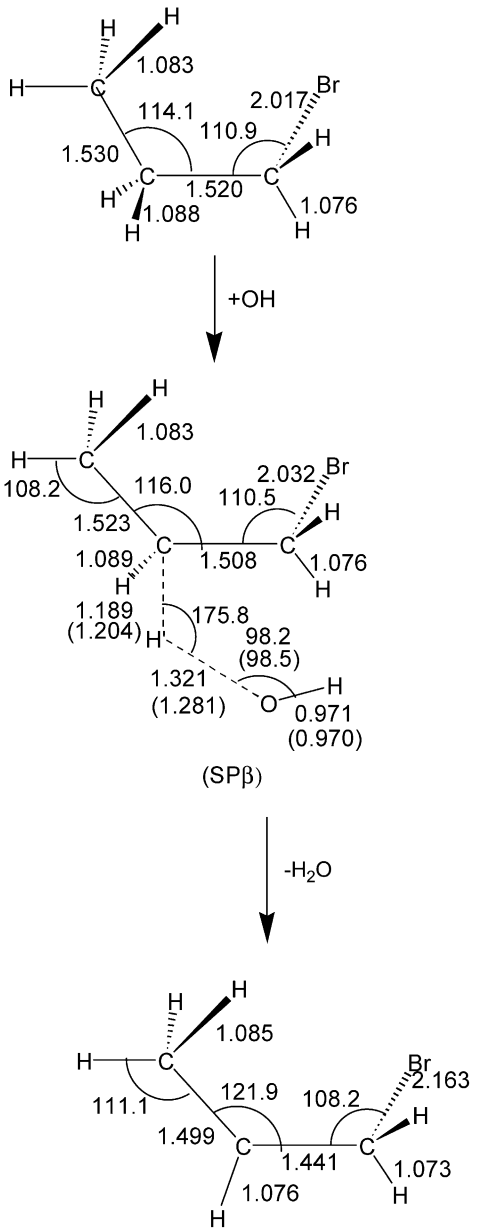

Fig. 5. Same as Fig. 3, but for the *gauche* without hydrogen bond conformer. Given in parentheses are the values at the MP2 = FULL/6-31G(d,p) level for the 'model' system, $CH_4 + OH$.

The more stable CR corresponds to the *gauche* conformation, while the more stable CP corresponds to the *anti* form, although it is necessary to note that the *gauche*–*anti* differences are very small, about 0.5 kcal mol^{-1}. As the temperature is an important factor affecting the stability of the complexes, we also calculated thermal corrections [TC($T \rightarrow 0$)] at temperatures in the range 298–2000 K, using standard methods of statistical thermodynamics. We found that the complexes of the R_α reaction disappear at $T \geq 700$ K, while the complexes of the R_β reaction (*gauche* with HB and *anti*) disappear at $T \geq 1000$ K.

Another important factor affecting the stability of the complexes is the basis set superposition error (BSSE). Note, however, that the definition of BSSE in the integrated method is unclear so that this factor was not calculated in the present work. Therefore, compared with other brominated complexes studied by our group [85], $CH_3 + HBr$ and $CH_2Br + HBr$, using non-integrated methods, we estimated this error to be about 1 kcal mol^{-1} at Level II, i.e. diminishing the real stability of the reactant and product complexes. Taking these last two factors (temperature and BSSE) into account simultaneously, at the Level II the complexes of the R_α reaction disappear at $T \geq 400\ K$, while the complexes of the R_β reaction (*gauche* with HB and *anti*) disappear at $T \geq 800\ K$. These results will permit us to analyse the possible change of mechanism with temperature.

With respect to the barrier heights, direct comparison with experiment is not possible. Raising the calculation level (Level 0 → Level II) lowers the barrier height drastically, 5–6 kcal mol^{-1}, and it may be expected that a more accurate barrier height would be obtained using highly correlated wave functions and larger basis sets. To obtain an estimate of our limitations, the IMOMO results are compared with the higher ab initio G3 barriers of Gilles et al. So, compared with the G3 values, our barriers at the Level II are overestimated by 0.90, 0.51 and 1.52 kcal mol^{-1} for the R_α, R_β (*anti*, the common saddle point studied in both works), and R_γ saddle points, respectively. Therefore, taking these differences in the barrier height and in the enthalpy of reaction (1 kcal mol^{-1}) as an estimate of the limitations of the Level II, the corrected barrier heights will be: 1.73 (R_α), 0.10 (R_β *gauche* with HB), 1.34 (R_β *gauche* without HB), 0.67 (R_β *anti*), and 3.61 (R_γ) kcal mol^{-1}. Note, however, that this is a general problem in computational chemistry, associated with the one-particle and *n*-particle basis set limitations, and is not directly related to the integrated methods used here.

3.3. Performance of the integrated method

In order to assess the performance of the integrated method, we compared our integrated results with ab initio benchmark calculations for the complete system [11]. Focussing the attention on the different saddle points (α,β,γ), first we compare the molecular geometry obtained with our integrated Level 0 [MP2 = FULL/6-31G(d,p): HF/6-31G] with those obtained by Gilles et al. [11] using the ab initio MP2 = FULL/6-31G(d) level by describing the complete system (Figs. 2, 4, and 6). Taking into account that in the integrated methods the complete system is divided into two parts which are described at different MO levels, it is necessary to distinguish between the parameters of the model system and the parameters of the rest of the system or outer layer. The integrated method gives a geometry similar to the high-level ab initio method for those parameters belonging to the model system, the most sensitive parameters being related to the breaking/forming bonds, C–H′ and O–H′, with differences of about 0.01 Å or less.

Table 2
Harmonic vibrational frequencies (cm^{-1}) and zero-point energy (ZPE, kcal mol^{-1}) for the R_β reaction (*gauche* with HB, *gauche* without HB and *anti* conformers) at the integrated Level 0. For comparison, values for the 'model' reaction $CH_4 + OH$ saddle point, independent of the IMOMO approach, optimised at the MP2 = FULL/6-31G(d,p) level are given in parentheses (See Section 3.5)

R	*Gauche* with HB		*Gauche* without HB		*Anti*			*P*
	CR_β	SP_β	CP_β	SP_β	CR_β	SP_β	CP_β	
3376	3826	3822(3845)	4017	3840	3833	3825	4020	3419
3297	3386	3381(3322)	3875	3392	3380	3378	3880	3334
3266	3305	3301(3318)	3441	3310	3299	3297	3442	3327
3262	3279	3278	3347	3273	3271	3269	3340	3253
3239	3273	3267	3340	3270	3264	3259	3330	3240
3191	3237	3197	3253	3230	3248	3235	3267	3177
3187	3200	3186(3177)	3241	3196	3195	3189	3244	1650
1656	3155	1660	3178	1658	3189	1654	3182	1644
1656	1665	1651	1710	1651	1657	1650	1710	1636
1636	1655	1625	1649	1630	1656	1629	1653	1580
1579	1629	1581(1545)	1645	1580	1635	1579	1648	1514
1565	1581	1536(1521)	1635	1477	1580	1528	1646	1332
1457	1555	1437(1465)	1581	1464	1576	1444	1588	1290
1419	1483	1390	1525	1391	1466	1376	1528	1216
1379	1418	1341(1327)	1336	1343	1426	1362	1348	1133
1355	1373	1285(1207)	1293	1290	1377	1312	1298	1120
1213	1337	1181	1210	1217	1353	1226	1215	971
1149	1191	1150	1135	1154	1214	1163	1139	913
1112	1155	1125	1107	1146	1152	1126	1110	638
970	1120	982	982	973	1107	994	985	430
930	970	965(940)	929	947	969	980	928	318
794	911	907	717	912	936	912	700	214
659	847	836	497	843	803	788	509	102
318	553	708(744)	436	640	641	655	451	84
247	523	550	362	551	387	621	344	
227	457	418	313	386	358	368	293	
116	419	388(356)	187	280	313	311	180	
	300	272(292)	153	204	248	248	154	
	220	211	108	152	226	225	133	
	154	168	92	99	140	143	113	
	138	129	79	80	123	129	92	
	86	84(31)	72	55	90	103	84	
	44	2015 i(2060 i)	47	1826 i	43	2014 i	56	
ZPE								
63.26	70.68	67.21	69.33	66.66	70.27	67.16	69.49	53.66

Obviously, these differences are larger for the rest of the system, due to the different MO description used with the two methods.

Second, we compare the barrier heights corrected for zero-point energy [$\Delta H^{\neq}(0\ K)$] obtained with our integrated Level II with those obtained by Gilles et al. using the ab initio Gaussian-3 (G3) method by describing the complete system. Taking into account the previous discussion in Section 3.2, our integrated values for the α, β(*anti*) and γ saddle points (Table 4): 1.70, 0.57 and 4.05 kcal mol^{-1}, show the same tendency as those obtained at the G3 level: 0.76, −0.21 and 2.72 kcal mol^{-1}, respectively.

These geometric and energetic results confirm the earlier conclusions from our group [54,55,60,61,86]. In general, integrated methods reproduce the properties obtained with the high-level method, correct the deficiencies of the lower-level method showing their effectiveness in correcting wrong potential energy surfaces, and represent a substantial saving in computational cost (memory and time) which is especially interesting for the study of large molecules.

3.4. Influence of the bromine atom description of the model system

In the case of the R_α reaction, due to that the bromine atom is a very computational demanding system, we test the possibility of substitute it by a link atom, hydrogen atom. Now the complete and model system are

$$^{\gamma}CH_3{}^{\beta}CH_2{}^{\alpha}CH_2Br + OH \rightarrow {}^{\gamma}CH_3{}^{\beta}CH_2{}^{\alpha}CHBr + H_2O \quad (R_\alpha)$$

$$^{\alpha}CH_4 + OH \rightarrow {}^{\alpha}CH_3 + H_2O \quad (R'_{m\alpha})$$

Note the difference with the $R_{m\alpha}$ model reaction previously analysed. While in that one there was one link atom,

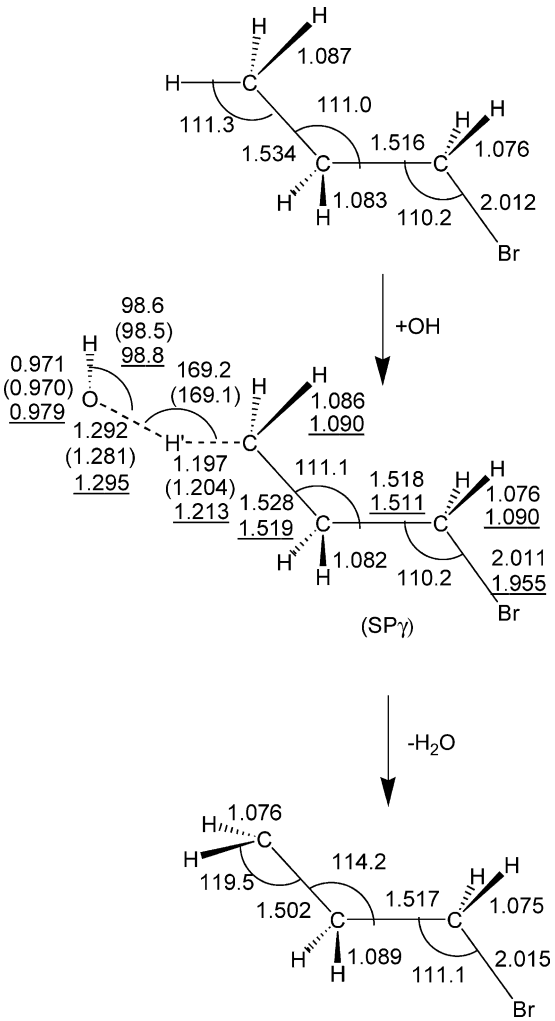

Fig. 6. Optimized stationary point geometries at Level 0 for the R_γ reaction. SP_γ, saddle point. H′ is the hydrogen being abstracted. Bonds in Å and angles in degrees. Given in parentheses are the values at the MP2 = FULL/6-31G(d,p) level for the 'model' system, CH_4 + OH. Underlined are the values for the 'complete' system at the MP2 = FULL/6-31G(d) level, from Ref. [11].

corresponding to the $^{\beta}C-^{\alpha}C$ bond, in this case there are two link atoms, corresponding to the original $^{\beta}C-^{\alpha}C$ and $^{\alpha}C-Br$ bonds.

As a test we used the energy of reaction. When the Br atom is included in the model reaction, this value is -14.92 kcal mol^{-1} (Table 4), while when it is excluded this value is -11.70 kcal mol^{-1}, making the comparison with experiment worse ($\Delta = 3.22$ kcal mol^{-1}). This result indicates that it is necessary to maintain the bromine atom for an adequate description of the reactive system, in spite of the computational effort demanded.

3.5. The model reaction

To help understand the influence of the description of the model reaction on the geometry, vibrational frequency, and energies of the IMOMO method, we choose the simplest case, $CH_4 + OH \rightarrow CH_3 + H_2O$ in the R_β and R_γ reactions. Figs. 3 and 5, and Tables 2 and 3 also present these magnitudes for the model reaction at the high-level MP2 = FULL/6-31G(d,p), for the respective R_β (*gauche*) and R_γ reactions.

First, for the saddle point geometry, the bond that is broken (C–H′) increases by only 11% in length and the bond that is formed (H′–O) by 33%. These increases agree with the results found for the saddle points in the R_β and R_γ reactions. Thus, this transition state is also early, which is consistent with the exothermicity of the model reaction (Table 4).

Second, the common frequencies in the model reaction (values in parentheses in Tables 2 and 3) and the complete system are in reasonable agreement. The imaginary frequency, 2060 i cm^{-1}, at the saddle point is close to the values in the complete systems (SP_β and $SP\gamma$).

Table 3
Harmonic vibrational frequencies (cm^{-1}) and zero-point energy (ZPE, kcal mol^{-1}) for the R_γ reaction at the integrated Level 0. For comparison, values for the 'model' reaction CH_4 + OH saddle point, independent of the IMOMO approach, optimised at the MP2 = FULL/6-31G(d,p) level are given in parentheses (See Section 3.5)

R_γ	SP_γ	P_γ
3376	3841(3845)	3406
3297	3377(3322)	3382
3266	3297(3318)	3304
3248	3284	3288
3236	3260	3185
3217	3229	3157
3150	3188(3177)	1634
1664	1659	1631
1636	1635	1550
1568	1541(1545)	1523
1566	1505(1521)	1431
1509	1488(1465)	1359
1485	1452	1266
1453	1382	1177
1383	1365	1129
1352	1308(1327)	1047
1199	1185(1207)	935
1151	1150	885
1106	1107	581
957	1039	529
922	923(940)	436
815	888	263
664	817	156
322	725(744)	141
248	646	
230	395(356)	
116	282(292)	
	235	
	123	
	83	
	72	
	54(31)	
	1999 i(2060 i)	
ZPE		
63.10	66.52	53.46

Table 4
Energy and enthalpy (0 and 298 K) changes relative to reactants (kcal mol^{-1}) for the three reactions at several integrated levels

	Level 0	Level I	Level II	GBGMR[a]	Exp.[b]	'Model reaction'[c]
R_α reaction						
CR_α	−6.42	−3.53	−3.76			
	−4.93	−2.04	−2.27			
	−4.55	−1.66	−1.89			
SP_α	8.71	5.71	3.63	2.73		
	6.78	3.78	1.70	0.76		
	6.71	3.71	1.63			
CP_α	−20.14	−18.89	−20.81			
	−19.62	−18.37	−20.29			
	−18.52	−17.27	−19.19			
P	−14.92	−15.80	−16.97			
	−15.84	−16.72	−17.89	−19.42		
	−15.41	−16.29	−17.46		−20.7 ± 1.3	
R_β reaction (gauche with HB)						
CR_β	−6.93	−6.14	−6.15			
	−5.01	−4.22	−4.23			
	−4.89	−4.10	−4.11			
SP_β	7.04	3.71	1.61			12.06
	5.49	2.16	0.06			10.34
	5.12	1.79	−0.31			10.00
CP_β	−27.05	−26.27	−23.47			
	−26.48	−25.70	−22.90			
	−25.38	−24.60	−21.80			
P	−19.03	−18.69	−17.59			−9.88
	−20.38	−20.04	−18.94			−11.58
	−19.75	−19.41	−18.31		−23.3 ± 2.1	−11.10
R_β reaction (gauche without HB)						
SP_β	8.81	5.37	2.85			12.06
	6.71	3.27	0.75			10.34
	6.75	3.31	0.79			10.00
P	−19.03	−18.68	−17.59			−9.88
	−20.38	−20.03	−18.94			−11.58
	−19.75	−19.40	−18.31			−11.10
R_β reaction (anti)						
CR_β	−6.03	−5.40	−5.22			
	−4.52	−3.89	−3.71			
	−4.16	−3.53	−3.35			
SP_β	7.32	3.99	2.18	1.67		12.06
	5.71	2.38	0.57	−0.21		10.34
	5.43	2.10	0.29			10.00
CP_β	−26.81	−26.44	−24.05			
	−26.08	−25.71	−23.32			
	−25.05	−24.68	−22.29			
P	−19.03	−18.69	−17.59			−9.88
	−20.38	−20.04	−18.94	−22.30		−11.58
	−19.75	−19.41	−18.31		−23.3 ± 2.1	−11.10
R_γ reaction						
SP_γ	11.01	7.60	6.13	4.61		12.06
	8.93	5.52	4.05	2.72		10.34
	8.96	5.55	4.08			10.00
P	−12.17	−12.09	−13.79			−9.88
	−13.56	−13.48	−15.18	−16.90		−11.58
	−13.19	−13.11	−14.81		−17.7 ± 1.0	−11.10

For each stationary point, the first entry corresponds to the energy change, the second to the enthalpy (0 K) change, and the third to the enthalpy (298 K) change, relative to reactants.

[a] Values of ΔH(0 K) from Ref. [11]. The values of ΔE have been obtained in the present work from the ΔH(0 K) and ZPE values taken from Ref. [11].

[b] Experimental enthalpy of reaction (298 K) from the following enthalpies of formation: $CH_3CH_2CH_2Br$: −20.8 ± 0.7 (Ref. [81]); OH: 9.4 (Ref. [82]); H_2O: −57.80 (Ref. [82]); CH_3CH_2CHBr: 25.7 ± 0.6 (Ref. [16]); CH_3CHCH_2Br: 23.1 ± 1.4 (Ref. [16]); $CH_2CH_2CH_2Br$: 28.7 ± 0.3 (Ref. [16]).

[c] For comparison, values for the 'model' reaction $CH_4 + OH$, independent of the IMOMO approach, optimised at the MP2 = FULL/6-31G(d,p) level.

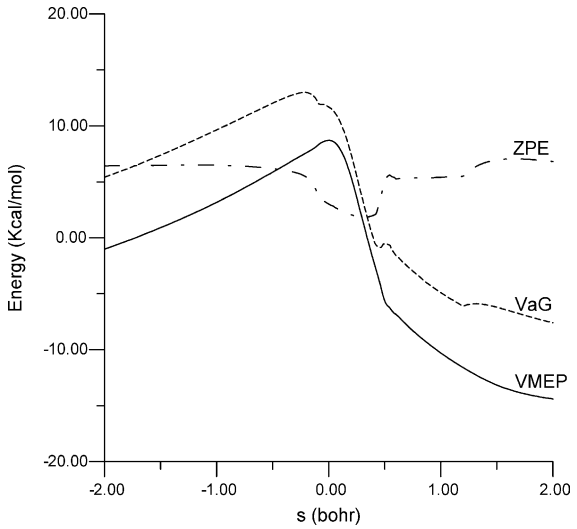

Fig. 7. Classical potential energy (V_{MEP}), vibrationally adiabatic potential energy (ΔV_a^G), and zero-point energy (ΔZPE) curves with respect to the reactants as a function of s for the R_α reaction at the Level 0, using curvilinear coordinates.

Third, with respect to the energy changes (reaction and activation) (Table 4) at similar levels, MP2 for the model reaction and Level 0 for the complete system, the behaviour is different depending on whether the reaction analysed is R_β or R_γ. While for the R_γ reaction the model reaction simulates the energy and enthalpy (0 and 298 K) changes of the complete system; for the R_β reaction the model system's results are very far of those for the complete system. Clearly, this different behaviour is related with the similarity (geometric and electronic) of the model and the complete reactions. As indicated in Section 2.1, in the R_β reaction two link atoms are necessary to ensure a saturated valence structure, while in the R_γ reaction only one is necessary. Moreover, this result justifies the choice of the R_γ reaction and the $CH_4 + OH$ model in the above discussion in Section 3.2 about the barrier height limitations.

Therefore, in the light of this comparison, it seems that the success of the IMOMO method is mainly due to the HL model system description, with the effects of the remaining LL fragments being smaller. This conclusion agrees with earlier studies by our group [54,55,60,61,86] using integrated methods.

3.6. Reaction-path analysis

Having analysed the mechanism of the three reactions, R_α, R_β, and R_γ, we shall now extend the IMOMO scheme to construct the corresponding reaction paths independently. The analyses of the reaction-paths were carried out on the information (energy, gradient, and Hessian) at the integrated Level 0 [MP2 = FULL/6-31G(d,p):HF/6-31G] over the s range -2.0 to $+2.0$ bohr, where the respective hydrogen-bonded complexes in the reactant and product channels have not yet been reached. Thus, the three hydrogen abstraction reactions present similar behaviour, and in this section only the R_α reaction is discussed to avoid unnecessary repetition.

The classical potential energy along the MEP, V_{MEP}, the ground-state vibrationally adiabatic potential energy, ΔV_a^G, and the change in the local zero-point energy, ΔZPE, curves as a function of s are shown in Fig. 7, and Fig. 8 shows some vibrational frequencies along the MEP. Note that ΔV_a^G and ΔZPE are defined as the difference between these magnitudes at s and their values for the reactants. The behaviour is that expected in hydrogen abstraction reactions, thus indicating the success of the integrated method in the description of this type of reaction. The mode related to the breaking (C–H′)/forming (H′–O) bonds presents a widening of the vibrational well, an effect which has been found in other reactions with a small skew angle

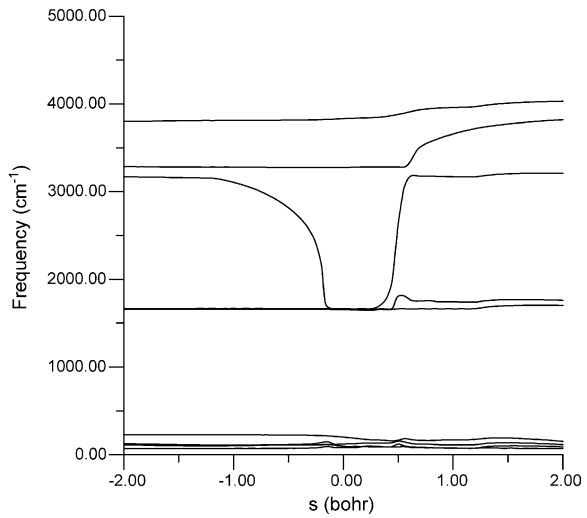

Fig. 8. Some generalized normal-mode vibrational frequencies plotted versus s for the R_α reaction at the Level 0. Note the widening and the drop of the reactive mode.

Table 5
Rate constant for the R_α reaction

T(K)	TST	CVT	SCT	CVT/SCT	Exp.[a]
200	1.15(−12)	1.46(−14)	4.96	7.20(−14)	
230	1.20(−12)	2.57(−14)	3.47	8.84(−14)	2.03(−13)
250	1.25(−12)	3.52(−14)	2.87	1.01(−13)	2.38(−13)
270	1.31(−12)	4.62(−14)	2.48	1.15(−13)	2.72(−13)
298	1.40(−12)	6.37(−14)	2.12	1.36(−13)	3.18(−13)
300	1.41(−12)	6.50(−14)	2.10	1.37(−13)	3.21(−13)
350	1.61(−12)	1.03(−13)	1.73	1.79(−13)	3.98(−13)
400	1.86(−12)	1.54(−13)	1.52	2.33(−13)	
500	2.51(−12)	2.74(−13)	1.31	3.61(−13)	
600	3.37(−12)	4.00(−13)	1.21	4.83(−13)	
1000	9.46(−12)	1.44(−12)	1.07	1.54(−12)	
1500	2.50(−11)	4.18(−12)	1.03	4.30(−12)	
2000	5.21(−11)	9.00(−12)	1.02	9.18(−12)	

The overall rate constants are obtained by multiplying the values for one approach of the OH radical by 4, corresponding to the two possibilities for the *gauche* and *anti* conformers. $\sigma = 4$ in Eq. (3). These scaled values correspond to Level 0×0.199, $\Delta E^{\neq} = 1.73$ kcal mol^{-1}.

[a] Ref. [11]. $k_\alpha(T) = 1.44 \cdot 10^{-12} \exp(-450/T)$, 230–360 K.

Table 6
Rate constant for the R_β reaction

T(K)	TST	CVT	SCT	CVT/SCT
Gauche with hydrogen-bond conformer				
200	1.02(−13)	3.62(−14)	1.83	6.61(−14)
230	1.08(−13)	4.35(−14)	1.60	6.91(−14)
250	1.11(−13)	4.80(−14)	1.49	7.17(−14)
270	1.14(−13)	5.27(−14)	1.41	7.45(−14)
298	1.19(−13)	6.00(−14)	1.33	7.94(−14)
300	1.20(−13)	6.05(−14)	1.33	7.98(−14)
350	1.53(−13)	7.06(−14)	1.23	8.73(−14)
400	1.71(−13)	8.46(−14)	1.17	9.97(−14)
500	2.16(−13)	1.15(−13)	1.11	1.29(−13)
600	2.77(−13)	1.51(−13)	1.07	1.63(−13)
1000	7.07(−13)	3.52(−13)	1.03	3.62(−13)
1500	4.12(−12)	8.15(−13)	1.01	8.25(−13)
2000	7.66(−12)	1.56(−12)	1.00	1.58(−12)
Gauche without hydrogen-bond conformer				
200	3.12(−12)	6.98(−15)	1.23	8.57(−15)
230	3.13(−12)	1.43(−14)	1.17	1.67(−14)
250	3.17(−12)	2.13(−14)	1.14	2.42(−14)
270	3.18(−12)	3.02(−14)	1.12	3.37(−14)
298	3.19(−12)	4.61(−14)	1.10	5.04(−14)
300	3.20(−12)	4.74(−14)	1.09	5.17(−14)
350	3.42(−12)	8.76(−14)	1.07	9.33(−14)
400	3.77(−12)	1.44(−13)	1.05	1.51(−13)
500	4.79(−12)	3.10(−13)	1.03	3.19(−13)
600	6.19(−12)	5.55(−13)	1.02	5.67(−13)
1000	1.64(−11)	2.45(−12)	1.00	2.46(−12)
1500	4.21(−11)	4.93(−12)	1.00	4.96(−12)
2000	8.65(−11)	1.13(−11)	1.00	1.14(−11)
Anti conformer				
200	1.52(−12)	2.88(−14)	2.62	7.54(−14)
230	1.53(−12)	4.04(−14)	2.11	8.50(−14)
250	1.62(−12)	4.90(−14)	1.89	9.26(−14)
270	1.63(−12)	5.82(−14)	1.74	1.01(−13)
298	1.76(−12)	7.20(−14)	1.58	1.14(−13)
300	1.90(−12)	7.30(−14)	1.57	1.15(−13)
350	2.22(−12)	1.01(−13)	1.40	1.41(−13)
400	2.63(−12)	1.33(−13)	1.30	1.72(−13)
500	3.20(−12)	2.10(−13)	1.18	2.48(−13)
600	3.55(−12)	2.98(−13)	1.12	3.34(−13)
1000	4.14(−12)	7.35(−13)	1.04	7.67(−13)
1500	9.55(−12)	1.88(−12)	1.02	1.92(−12)
2000	1.85(−11)	3.82(−12)	1.01	3.84(−12)

Total rate constant for the R_β reaction[a]

T(K)	CVT/SCT	Exp.[b]
200	1.50(−13)	
230	1.71(−13)	4.25(−13)
250	1.88(−13)	4.58(−13)
270	2.09(−13)	4.94(−13)
298	2.44(−13)	5.49(−13)
300	2.46(−13)	5.53(−13)
350	3.22(−13)	6.63(−13)
400	4.23(−13)	
500	6.96(−13)	
600	1.06(−12)	
1000	3.59(−12)	
1500	7.70(−12)	
2000	1.68(−11)	

For the *gauche* conformers (with and without hydrogen-bond) there is only one abstractable hydrogen. Thus, the overall rate constants are obtained independently with a symmetry factor of 1. For the *anti* conformer, $\sigma = 2$, in accordance with the two possibilities of the hydrogen abstraction reaction. These scaled values correspond to Level 0 by the corresponding scale factor.

[a] k(total) = k(*gauche* with HB) + k(*gauche* without HB) + k(*anti*).

[b] The experimental value is taken from Ref. [11], $k_\beta(T) = 2.54{\cdot}10^{-18}T^2 \exp(+265/T)$, over the temperature range 230–360 K, and it corresponds to the overall rate constants including the *gauche* and *anti* conformers.

[60,87–89]. This mode drops sharply near the saddle point (*reactive mode*), and as a result the ZPE shows noticeable changes with s (Fig. 7).

3.7. Improved reaction-paths

The poor energy description with the integrated Level 0 (see Section 3.2 and Table 4) means that the integrated reaction-paths have to be optimized. In previous work [88,90,91] we analysed different approximations to scale the complete path, and based on this experience we decided to scale the original curve (MP2:HF Level 0) uniformly by a factor

$$f = \Delta E^{\neq}(\text{Corrected-Level II},\ s = 0)/\Delta E^{\neq}\ (\text{Level 0},\ s = 0)$$

where $\Delta E^{\neq}$ is the variation of energy at each level with respect to the reactants. At the saddle point, $s = 0$, the barrier height is that of the highest level, corrected-Level II in each case. These factors are: 0.199, 0.014, 0.152, 0.091 and 0.328 for R_α, R_β (*gauche* with HB), R_β (*anti*), R_β (*gauche* without HB), and R_γ, respectively. Therefore, the rate constants obtained with this method will be denoted scaled-values.

3.8. Rate constants

The bottleneck properties, based on the CVT approach, show that the location of the generalized transition state (GTS) is away from the saddle point: from −0.279 to −0.163 for the R_α reaction, from −0.356 to −0.183 for the R_β (*anti*) reaction, and from −0.444 to −0.157 for the R_γ reaction, over the temperature range 200–2000 K. Thus the variational effects, i.e. the ratio between the variational CVT and conventional TST rate constants, are important for these reactions. This result agrees with the behaviour of the model system, $CH_4 + OH$, [80,92,93] and with the behaviour found in our group's earlier work [60,61].

In Tables 5–7 the calculated conventional TST and variational CVT rate constants at the scaled-level, in the temperature range 200–2000 K, for the R_α, R_β and R_γ reactions are compared to experimental values [11,12,14] in the common temperature range. First, due to the low barrier heights, the tunnelling effect is few important for these reactions, ranging from 4.96 to 1.52 over the temperature range 200–400 K. Second, in the common temperature range 230–350 K, the theoretical results underestimate the experimental data. For instance, at 298 K, these factors are 2.3, 2.2 and 8.0 for the R_α, R_β, and R_γ reactions, respectively. This discrepancy can be explained if two effects are considered: the barrier height and the tunnelling

Table 7
Rate constant for the R_γ reaction

T(K)	TST	CVT	SCT	CVT/SCT	Exp.[a]
200	4.13(−14)	4.11(−16)	1.88	7.76(−16)	
230	8.24(−14)	1.50(−15)	1.59	2.37(−15)	4.50(−14)
250	1.21(−13)	3.00(−15)	1.47	4.43(−15)	6.29(−14)
270	1.69(−13)	5.42(−15)	1.39	7.54(−15)	8.35(−14)
298	2.56(−13)	1.10(−14)	1.30	1.44(−14)	1.16(−13)
300	2.64(−13)	1.15(−14)	1.30	1.50(−14)	1.19(−13)
350	4.85(−13)	2.59(−14)	1.21	3.14(−14)	1.88(−13)
400	8.00(−13)	5.65(−14)	1.15	6.54(−14)	
500	1.78(−12)	1.70(−13)	1.10	1.95(−13)	
600	3.35(−12)	3.46(−13)	1.06	3.69(−13)	
1000	1.86(−11)	2.69(−12)	1.02	2.75(−12)	
1500	6.98(−11)	1.17(−11)	1.01	1.18(−11)	
2000	1.73(−10)	3.11(−11)	1.00	3.12(−11)	

The overall rate constants are obtained by multiplying the values for one approach of the OH radical by 3, corresponding to the three possibilities of the hydrogen abstraction reaction. $\sigma = 3$ in Eq. (3). These scaled values correspond to Level 0×0.328, $\Delta E^{\neq} = 3.61$ kcal mol^{-1}.

[a] Ref. [11]. $k_\gamma(T) = 2.89{\cdot}10^{-12} \exp(-957/T)$, 230–360 K.

effect of large curvature (LC). As it was indicated in Section 3.2 by analysing the barrier height, higher correlated wavefunctions and larger basis sets are necessary to continue lowering the barrier. In this direction, Masgrau and coworkers [80] pessimistically reported that, even though they used the highest ab initio electronic level reported up to now for dynamics calculations of the $CH_4 + OH$ reaction, the experimental rate constants were not reproduced exactly. With respect to the second factor, as we indicated above, the LC method requires more information about other zones of the PES than was determined in this study. However, this effect can be estimated by considering the model reaction $CH_4 + OH$.

Table 8
Total rate constants for the $CH_3CH_2CH_2Br + OH$ reaction

T(K)	CVT/SCT[a]	Exp.[b]	Exp.[c]	Exp.[d]
200	2.23(−13)			
230	2.62(−13)	6.97(−13)	6.82(−13)	7.22(−13)
250	2.94(−13)	7.68(−13)	7.64(−13)	8.01(−13)
270	3.32(−13)	8.36(−13)	8.52(−13)	8.90(−13)
298	3.94(−13)	9.27(−13)	9.82(−13)	1.03(−12)
300	4.00(−13)	9.34(−13)	9.92(−13)	1.04(−12)
350	5.32(−13)	1.09(−12)	1.25(−12)	1.34(−12)
400	7.20(−13)	1.23(−12)	1.55(−12)	1.71(−12)
500	1.25(−12)			2.65(−12)
600	1.92(−12)			
1000	7.88(−12)			
1500	2.38(−11)			
2000	5.27(−11)			

[a] Theoretical overall scaled rate constants from this work.
[b] Ref. [14]. $k(T) = 9.1{\cdot}10^{-14} T^{0.5} \exp(-157/T)$, 220 − 380 K.
[c] Ref. [11]. $k(T) = (6.6 \pm 0.5)10^{-18} T^2 \exp(+154/T)$, 230–360 K.
[d] Ref. [12]. $k(T) = 2.99{\cdot}10^{-13} (T/298)^{2.79} \exp(+369/T)$, 210–480 K.

We obtained [93] a factor LC/SCT ranging from 1.5 to 1.1 over the temperature range 250–500 K.

As was shown in the analysis, the title reaction can proceed via three pathways which compete with each other. Therefore, the total rate constant will be

$$k(T) = k_\alpha(T) + k_\beta(T) + k_\gamma(T) \quad (4)$$

where the symmetry factors are included in the respective $k(T)$. Table 8 lists the theoretical scaled total rate constants (obtained from the partial results in Tables 5–7) for the temperature range 200–2000 K together with the experimental values [11,12,14] for comparison.

First, for the common range of temperatures (200–500 K) the experimental and theoretical total rate constants showed a slight curvature of the Arrhenius plot, which was more evident when a larger range of temperatures was considered. Clearly, this is the expected behaviour in a reaction with a heavy–light–heavy mass combination, due to the tunneling effect. Second, in accordance with the individual rate constants, the total theoretical values underestimate the experimental determinations [11,12,14] by factors from 2.60 to 2.15 over all the common temperature range (230–400 K). Third, at low temperatures (atmosphere) the R_β reaction is the most important, while at high temperatures (combustion) the influence of the R_γ reaction increases, indicating clearly a change of the abstraction site with temperature.

The activation energy can be obtained from the total rate constants through the usual definition

$$E_a = -R[\mathrm{d}(\ln k)/\mathrm{d}(1/T)] \quad (5)$$

which is equivalent to determining the slope of the Arrhenius plot. The values for the scaled-level scheme are: 0.94 kcal mol^{-1} in the range 230–350 K; 1.14 kcal mol^{-1} in the range 200–500 K; and 4.21 kcal mol^{-1} at high temperatures, 600–1000 K. At the lowest temperatures, those of atmospheric interest, the theoretical values show reasonable agreement with the experimental data: 0.65 (210–480 K) [12] and 0.61 ± 0.14 (230–386 K) [14] kcal mol^{-1}. Unfortunately, at higher temperatures there is no experimental information for comparison.

From the kinetics information in Tables 5–8 one can obtain the branching ratios (Table 9). Taking into account the experimental error bars, the agreement between theory and experiment is reasonable, overestimating the R_α and R_β reactions, and underestimating the R_γ reaction. More interesting is the variation of the branching ratios with temperature. While the influence of the R_α and R_β reactions decreases with temperature, the weight of the R_γ reaction increases. Thus, R_γ surpasses R_α at 1000 K and R_β at 1500 K. Thus, the direct reaction, without intermediate complexes, is favoured by increasing temperature, as we had concluded from analysing the stability of the complexes of the R_α and R_β reactions.

Table 9
Branching ratios for the title reaction

T(K)	k_α/k_T		k_β/k_T		k_γ/k_T	
	Theo.[a]	Exp.[b]	Theo.	Exp.	Theo.	Exp.
200	0.32		0.67		0.01	
230	0.33	0.30 ± 0.08	0.65	0.61 ± 0.02	0.02	0.08 ± 0.08
250	0.33	0.31 ± 0.07	0.64	0.60 ± 0.02	0.03	0.09 ± 0.07
270	0.34	0.31 ± 0.06	0.63	0.58 ± 0.02	0.03	0.11 ± 0.06
298	0.34	0.32 ± 0.04	0.62	0.56 ± 0.02	0.04	0.12 ± 0.04
300	0.34	0.32 ± 0.04	0.62	0.56 ± 0.02	0.04	0.12 ± 0.04
350	0.34	0.32 ± 0.02	0.60	0.52 ± 0.02	0.06	0.16 ± 0.02
400	0.32		0.59		0.09	
500	0.29		0.55		0.16	
600	0.25		0.54		0.21	
1000	0.20		0.45		0.35	
1500	0.18		0.32		0.50	
2000	0.16		0.29		0.55	

[a] Theoretical values from this work using the scaled rate constants.
[b] Experimental values from Ref. [11]. At 298 K, using the empirical structure–reactivity relationship of Atkinson [94] the branching ratios are: 0.35, 0.47 and 0.18, respectively.

3.9. Tropospheric lifetimes

The compound *n*PB is regarded as a candidate to replace CFCs because of its short lifetime in the atmosphere. The main process in its removal from the atmosphere is the reaction with hydroxyl radicals.

To estimate its lifetime in the troposphere (characteristic temperatures in the range 215–300 K), two approximations were used. In the simplest approximation [95,96], the tropospheric residence time is given by

$$\tau_n\mathrm{PB} = (k_{n\mathrm{PB}}\cdot[\mathrm{OH}])^{-1} \quad (6)$$

where $[\mathrm{OH}] = 1.1 \times 10^6$ molecules cm^{-3} [97]. With this work's rate constant calculated at 277 K (3.42×10^{-13} $\mathrm{cm}^3\mathrm{molecule}^{-1}\mathrm{s}^{-1}$), the calculated lifetime was 31 days. With the more sophisticated model of Prather and Spivakovsky [98], the lifetime is

$$\tau_{n\mathrm{PB}} = [k_{\mathrm{MC}}(277)/k_{n\mathrm{PB}}(277)].\tau_{\mathrm{MC}} \quad (7)$$

where $k_{\mathrm{MC}}(277)$ and τ_{MC} are the rate constant at 277 K (6.71×10^{-15} $\mathrm{cm}^3\mathrm{molecule}^{-1}\mathrm{s}^{-1}$) and the corrected lifetime (5.7 years ≈ 2052 days) of the methylchloroform (MC) reference, respectively. With this work's rate constant at 277 K, the calculated lifetime was 40 days. These theoretical estimates (31 and 40 days) are greater than the experimental estimations, which agrees with the underestimation of the calculated rate constants. So, these estimations can be considered only as an upper limit.

4. Conclusions

This work has attempted to shed some light on the mechanism and kinetics of the reaction of *n*-propyl bromide with free OH radicals in the gas phase, at low (atmosphere) and high (combustion) temperatures, using ab initio integrated methods.

First, the OH radical attacks *n*PB at the three carbons, α, β, and γ, in a competitive manner and with different hydrogen abstraction pathways. Thus, at low temperatures the pathways at the carbons α (which supports the bromine atom) and β (secondary carbon) proceed via hydrogen-bonded complexes in the entrance and exit channels, while at higher temperatures both proceed directly without intermediate complexes. The pathway at the γ carbon proceeds directly without intermediate complexes over all the temperature range.

Second, the kinetics of the reaction was analysed and the intrinsic reaction paths for each OH approach were constructed independently. With this information the rate constants were independently calculated using variational transition-state theory with small curvature multidimensional tunneling, where the reaction-path was scaled to higher levels of calculation using the single-point calculation technique. Even at high ab initio levels, the present theoretical results underestimate the experimental values.

Third, the total and partial rate constants show curvature of the Arrhenius plots, in accordance with the experimental data, indicating the importance of the tunneling effect. At low temperatures (atmosphere) the theoretical results show a reasonable agreement with the experimental data, and this permits us to assume that the behaviour could be similar at high temperatures (combustion) for which there are no experimental data.

Fourth, the analysis of the branching ratios showed a change of the abstraction site with temperature. Thus, at low temperatures the R_β reaction predominates, while at high temperatures the R_γ reaction is the most important.

Acknowledgements

We are grateful to Prof. Donald G. Truhlar for providing a copy of the GAUSSRATE program, and to the Consejeria de Educación, Ciencia y Tecnología, Junta de Extremadura (Spain) (Project No. 2PR01A002) for partial financial support of this work

References

[1] D.L. Albritton, R.T. Watson, Methyl bromide: its atmospheric science, technology and economics, Montreal Protocol Assessment Supplement, UNEP, Nairobi, Kenya, 1993.
[2] D.L. Albritton, R.T. Watson, P.J. Aucamp, Scientific Assesment of Ozone Depletion:, 1994, World Meteorological Organization, Global Ozone Research and Monitoring Project—Report No. 37, WMO, Geneva, 1995.
[3] G. Le Bras, U. Platt, Geophys. Res. Lett. 22 (1995) 599.
[4] M. Hausmann, U. Platt, J. Geophys. Res. 99 (1994) 25399.
[5] A. Bierbach, I. Barnes, K.H. Becker, Int. J. Chem. Kinet. 28 (1996) 565.

[6] T. Donaghy, I. Shanahan, M. Hande, S. Fitzpatrick, Int. J. Chem. Kinet. 25 (1993) 273.
[7] J.D.D. Nelson, J.C. Wormhoudt, M.S. Zahniser, C.E. Kolb, M.K.W. Ko, D.K. Weisenstein, J. Chem. Phys. 101 (1997) 4987.
[8] D.J. Wuebbles, A.K. Jain, K.O. Patten, Atmos. Environ. 32 (1998) 107.
[9] C.H. Bridgeman, J.A. Pyle, D.E. Shallcross, J. Geophys. Res. Atmos. 105 (2000) 26493.
[10] D.J. Wuebbles, K.O. Patten, M.T. Johnson, R. Kotamarthi, J. Geophys. Res. 106 (2001) 14.
[11] M.K. Gilles, J.B. Burkholder, T. Gierczak, P. Marshall, A.R. Ravishankara, J. Phys. Chem. A 106 (2002) 5358.
[12] S.N. Kozlov, V.L. Orkin, R.E. Huie, M.J. Kurylo, J. Phys. Chem. A 107 (2003) 1333.
[13] S. Téton, A.E. Boudali, A. Mellouki, J. Chim. Phys. 93 (1996) 274.
[14] S.C. Herndon, T. Gierczak, R.K. Talukdar, A.R. Ravishankara, Phys. Chem. Chem. Phys. 3 (2001) 4529.
[15] V.L. Orkin, S.N. Kozlov, F.J. Louis, R.E. Huie, M.J. Kurylo, Atmospheric Fate of Some Short-Lived Br Containing Hydrohalocarbons: OH Reactions and UV Spectra, Workshop on Laboratory Studies of Upper Troposphere/Lower Stratosphere Precesses, Breckenridge, CO, 2001.
[16] J. Espinosa-García, Chem. Phys. Lett. 377 (2003) 607.
[17] L.A. Curtiss, K. Raghavachari, P.C. Redfern, V. Rassolov, J.A. Pople, J. Chem. Phys. 109 (1998) 7764.
[18] L.A. Curtiss, P.C. Redfern, V. Rassolov, G. Kedziora, J.A. Pople, J. Chem. Phys. 114 (2001) 9998.
[19] R.G. Parr, W. Yang, Density Functional Theory of Atoms and Molecules, Oxford University Press, New York, 1989.
[20] R.M. Dreizler, E.K.U. Gross, Density Functional Theory, Springer, Berlin, 1990.
[21] J.K. Labanowski, J.E. Andzelm (Eds.), Density Functional Theory in Chemistry, Springer, Berlin, 1991.
[22] L.J. Bartolotti, K. Flurchick, in: K.B. Lipkowitz, D.B. Boyd (Eds.), Reviews in Computational Chemistry, vol. 7, VCH, 1996, p. 187.
[23] A. St Amant, in: K.B. Lipkowitz, D.B. Boyd (Eds.), Reviews in Computational Chemistry, vol. 7, VCH, 1996, p. 217.
[24] T. Ziegler, Chem. Rev. 91 (1991) 651.
[25] C.W. Bauslicher, Chem. Phys. Lett. 246 (1995) 40.
[26] P.C. Redfern, P. Zapol, L.A. Curtiss, K. Raghavachari, J. Chem. Phys. 104 (2000) 5850.
[27] B.G. Johnson, C. González, P.M.W. Gill, J.A. Pople, Chem. Phys. Lett. 221 (1994) 100.
[28] M.R. Pederson, Chem. Phys. Lett. 230 (1994) 54.
[29] D. Porezag, M.R. Pederson, J. Chem. Phys. 102 (1995) 9345.
[30] J.L. Durant, Chem. Phys. Lett. 256 (1996) 595.
[31] B.S. Jursic, Chem. Phys. Lett. 264 (1997) 113.
[32] S. Skokov, R.A. Wheeler, Chem. Phys. Lett. 271 (1997) 251.
[33] D.J. Tozer, N.C. Handy, J. Phys. Chem. 102 (1998) 3162.
[34] E. Proynov, H. Chermette, D.R. Salahub, J. Chem. Phys. 113 (2000) 10021.
[35] B.J. Lynch, D.G. Truhlar, J. Phys. Chem. 105 (2001) 2936.
[36] A. Warshel, M. Levitt, J. Mol. Biol. 103 (1976) 227.
[37] U.C. Singh, P.A. Kollman, J. Comp. Chem. 7 (1986) 718.
[38] M.J. Field, P.A. Bash, M. Karplus, J. Comp. Chem. 11 (1990) 700.
[39] J. Eckert, G.J. Kubas, J.H. Hall, P.J. Hay, C.M. Boyle, J. Am. Chem. Soc. 112 (1990) 2324.
[40] A. Warshel, Computer Modeling of Chemical Reactions in Enzymes and Solutions, Wiley, New York, 1991.
[41] H. Kawamura, N. Koga, K. Morokuma, J. Am. Chem. Soc. 114 (1992) 8687.
[42] F. Maseras, N. Koga, K. Morokuma, Organometallics 13 (1994) 4008.
[43] F. Maseras, K. Morokuma, J. Comp. Chem. 16 (1995) 1170.
[44] S. Humbel, S. Sieber, K. Morokuma, J. Chem. Phys. 105 (1996) 1959.
[45] M. Svensson, S. Humbel, K. Morokuma, J. Chem. Phys. 105 (1996) 3654.
[46] M. Svensson, S. Humbel, R.D.J. Froese, T. Matsubara, S. Sieber, K. Morokuma, J. Phys. Chem. 100 (1996) 19357.
[47] E.L. Coitiño, D.G. Truhlar, K. Morokuma, Chem. Phys. Lett. 259 (1996) 159.
[48] E.L. Coitiño, D.G. Truhlar, J. Phys. Chem. 101 (1997) 4641.
[49] M. Noland, E.L. Coitiño, D.G. Truhlar, J. Phys. Chem. 101 (1997) 1193.
[50] J. Gao, Rev. Comput. Chem. 7 (1996) 119.
[51] J.C. Corchado, D.G. Truhlar, J. Phys. Chem. 102 (1998) 1895.
[52] J.C. Corchado, D.G. Truhlar, in: J. Gao, M.A. Thompson (Eds.), Combined Quantum Mechanical and Molecular Mechanical Methods, ACS Symposium Series, vol. 712, ACS, Washington, DC, 1998, p. 106.
[53] S. Dapprich, I. Komaromi, K.S. Byun, K. Morokuma, M.J. Frisch, J. Mol. Struct. (Theohem) 461 (1999) 1.
[54] J. Espinosa-García, J.C. Corchado, J. Chem. Phys. 115 (2001) 3021.
[55] J. Espinosa-García, Phys. Chem. Chem. Phys. 4 (2002) 1807.
[56] Y. Zhang, H. Liu, W. Yang, J. Chem. Phys. 112 (2000) 3483.
[57] T.N. Truong, W.T. Duncan, A. Tirtowidjojo, Phys. Chem. Chem. Phys. 1 (1999) 1061.
[58] T.N. Truong, T.T. Truong, Chem. Phys. Lett. 314 (1999) 529.
[59] T.N. Truong, D.K. Maity, T.T. Truong, J. Chem. Phys. 112 (2000) 24.
[60] J. Espinosa-García, J. Phys. Chem. A 106 (2002) 5686.
[61] J. Espinosa-García, J. Phys. Chem. A 107 (2003) 1618.
[62] M.J. Frisch, G.W. Trucks, H.B. Schlegel, E. Scuseria, M.A. Robb, J.R. Cheeseman, V.G. Zakrzewski, J.A. Montgomery, R.E. Stratman, J.C. Burant, S. Dapprich, J.M. Millam, A.D. Daniels, K.N. Kudin, M.C. Strain, O. Farkas, J. Tomasi, V. Barone, M. Cossi, R. Cammi, B. Menucci, C. Pomelli, C. Adamo, S. Clifford, J. Ochterki, G.A. Petterson, P.Y. Ayala, Q. Cui, K. Morokuma, D.K. Malik, A.D. Rabuk, K. Raghavachari, J.B. Foresman, J. Cioslowski, J.V. Ortiz, J. J. Stefanov, G. Liu, A. Liashenko, P. Piskorz, I. Komaromi, R. Gomperts, R.L. Martin, D.J. Fox, T. Keith, M.A. Al-Laham, C.Y. Peng, A. Nanayakkara, C. González, M. Challacombe, P.M.W. Gill, B.G. Johnson, W. Chen, M.W. Wong, J.L. Andres, M. Head-Gordon, E.S. Reploge, J.A. Pople, GAUSSIAN98 program, Revision A.7, Gaussian Inc., Pittsburg, PA 1998.
[63] R.J. Bartlett, J. Phys. Chem. 93 (1989) 1697.
[64] A.D. Isaacson, D.G. Truhlar, J. Chem. Phys. 76 (1982) 1380.
[65] W.H. Miller, N.C. Handy, J.E. Adams, J. Chem. Phys. 72 (1980) 99.
[66] D.G. Truhlar, A.D. Isaacson, B.C. Garrett, in: M. Baer (Ed.), The Theory of Chemical Reactions, Chemical Rubber, Boca Raton, FL, 1985, p. vol. 4.
[67] B.C. Garrett, D.G. Truhlar, J. Am. Chem. Soc. 101 (1979) 4534.
[68] J.C. Corchado, E.L. Coitiño, Y.-Y. Chuang, D.G. Truhlar, GAUSSRATE, Version 8.0/P8.0-G94, University of Minnesota, Minneapolis, MN, 1998.
[69] Y.-Y. Chuang, J.C. Corchado, P.L. Fast, J. Villá, E.L. Coitiño, W.P. Hu, Y.P. Liu, G.C. Lynch, K. Nguyen, C.F. Jackells, M.Z. Gu, I. Rossi, S. Clayton, V. Melissas, R. Steckler, B.C. Garrett, A.D. Isaacson, D.G. Truhlar, POLYRATE Version 8.4, University of Minnesota, Minneapolis, 1999.
[70] D.G. Truhlar, J. Comput. Chem. 12 (1991) 266.
[71] C.F. Jackels, Z. Gu, D.G. Truhlar, J. Chem. Phys. 102 (1995) 3188.
[72] Y.Y. Chuang, D.G. Truhlar, J. Phys. Chem. 101 (1997) 3808.
[73] G.A. Natanson, B.C. Garrett, T.N. Truong, T. Joseph, D.G. Truhlar, J. Chem. Phys. 94 (1991) 7875.
[74] J. Espinosa-García, J. Corchado, J. Phys. Chem. 100 (1996) 16561.
[75] D.h. Lu, T.N. Truong, V.S. Melissas, G.C. Lynch, Y.P. Liu, B.C. Garrett, R. Steckler, A.D. Isaacson, S.N. Rai, G.C. Hancock, T. Lauderdale, D.G. Joseph, Comput. Phys. Commun. 71 (1992) 235.
[76] T.N. Truong, D.h. Lu, G.C. Lynch, Y.P. Liu, V.S. Melissas, J.J. Stewart, R. Steckler, B.C. Garrett, A.D. Isaacson, A. González-Lafont, S.N. Rai, G.C. Hancock, T. Joseph, D.G. Truhlar, Comput. Phys. Commun. 75 (1993) 43.
[77] G.S. Hammond, J. Am. Chem. Soc. 77 (1955) 334.
[78] H. Basch, S. Hoz, J. Phys. Chem. 101 (1997) 4416.

[79] M.D. Wheeler, M. Tsiouris, M. Laster, G. Lendvay, J. Chem. Phys. 112 (2000) 6590.
[80] L. Masgrau, A. González-Lafont, J.M. Lluch, J. Chem. Phys. 114 (2001) 2154.
[81] J.B. Pedley, R.D. Naylor, S.P. Kirby, Thermochemical Data of Organic Compounds, second ed., Chapman & Hall, New York, 1986.
[82] JANAF Thermochemical Tables, in: M.W. Chase, C.A. Davies, J.R. Downey, D.J. Frurip, R.A. McDonald, A.N. Syverud (Eds.), National Standard Reference Data Series, Third ed., vol. 14, National Bureau of Standards, Washington, DC, 1985.
[83] D.A. Dixon, D. Feller, J. Phys. Chem. A 102 (1998) 8209.
[84] P.L. Fast, J.C. Corchado, M.L. Sánchez, D.G. Truhlar, J. Phys. Chem. A 103 (1999) 3139.
[85] J. Espinosa-García, Mol. Phys. 97 (1999) 629.
[86] J. Espinosa-García, Trends in Chemical Physics 10 (2002) 31.
[87] D.K. Bondi, J.N.L. Connor, B.C. Garrett, D.G. Truhlar, J. Chem. Phys. 78 (1983) 5981.
[88] J. Espinosa-García, J.C. Corchado, J. Chem. Phys. 101 (1994) 8700.
[89] J. Espinosa-García, E.L. Coitiño, A. González-Lafont, J.M. Lluch, J. Phys. Chem. 102 (1998) 10715.
[90] J. Espinosa-García, J.C. Corchado, J. Chem. Phys. 101 (1994) 1333.
[91] J. Espinosa-García, J. Phys. Chem. A 104 (2000) 7537.
[92] V.S. Melissas, D.G. Truhlar, J. Chem. Phys. 99 (1993) 1013.
[93] J. Espinosa-García, J.C. Corchado, J. Chem. Phys. 112 (2000) 5731.
[94] R. Atkinson, Handbook of Property Estimation Methods for Chemical Environmental and Health Sciences, CRC Press LLC, Boca Raton, FL, 2000.
[95] J.S. Francisco, J. Chem. Phys. 96 (1992) 7597.
[96] R. Atkinson, Chem. Rev. 85 (1985) 192.
[97] B.R. Miller, J. Huang, R.F. Weiss, R.G. Prinn, P.J. Fraser, J. Geophys. Rev. 103 (1998) 13237.
[98] M. Prather, C.M. Spivakovsky, Geophys. Res. 95 (1990) 723.